Passive Seismic Characterization of High Priority Salt Jugs in Hutchinson, Kansas: August 2024

Shelby L. Peterie, Julian Ivanov, Marcus Tamburro, Richard D. Miller, Brett C. Bennett, Brett Wedel, Robbie Kieffer, Connor Umbrell, Cole Bunker, Carl Gonzales, and Max Zabinski

Kansas Geological Survey
1930 Constant Avenue
Lawrence, KS 66047

Draft Report to

Dale Davis and Spencer Cronin
Burns & McDonnell
9400 Ward Parkway
816-839-9526

Open-File Report 2025–47 April 2025

The Kansas Geological Survey makes no warranty or representation, either express or implied, with regard to the data, documentation, or interpretations or decisions based on the use of this data including the quality, performance, merchantability, or fitness for a particular purpose. Under no circumstances shall the Kansas Geological Survey be liable for damages of any kind, including direct, indirect, special, incidental, punitive, or consequential damages in connection with or arising out of the existence, furnishing, failure to furnish, or use of or inability to use any of the database or documentation whether as a result of contract, negligence, strict liability, or otherwise. This study was conducted in complete compliance with ASTM Guide D7128-05. All data, interpretations, and opinions expressed or implied in this report and associated study are reasonably accurate and in accordance with generally accepted scientific standards.

Passive Seismic Characterization of High Priority Salt Jugs in Hutchinson, Kansas: August 2024

Executive Summary

This project appraised changes in stress conditions of rock above selected dissolution voids by estimating the relative stress field from the calculated shear-wave velocity of the overburden. An estimate of change and potential risk each void represents can be estimated by comparing the current stress conditions with those measured in previous surveys. Shear-wave velocities were calculated using passive surface-wave methods. Data were acquired along thirteen profiles located on or near key abandoned brine production wells using train traffic as an energy source. The multichannel analysis of surface waves (MASW) method provided an estimate of the shear-wave velocity, at a resolution sufficient to loosely map the alluvial/bedrock contact and velocity characteristics of the Permian-aged Ninnescah Shale above the top of the "three finger" dolomite (at approximately 100 m below ground surface). A key outcome was the differentiation of relative rock stress based on shear velocity above solution mining caverns (salt jugs, associated with the target wells) compared to rocks above undisturbed salt or jugs reported without wide spans of unsupported roof rock. Comparisons of shear-wave velocity profiles over time (timelapse) provided insights into consistency of overburden stability and therefore indirectly, void dynamics.

Passive MASW data were continuously acquired over four nights (August 12-15, 2024) above wells with a potential to impact surface access or assets or with production histories consistent with past cases of void migration on the Vigindustries site in Hutchinson, Kansas. A continuous sampling approach targeting different wells each night was used to record all available train sources of passive source energy to maximize opportunities to capture energy with optimal source orientation and surface-wave characteristics. Surface waves were recorded with frequencies as low as 4.5 Hz, representing an approximately 60 m average maximum depth of investigation, and used to map bedrock velocity of at least the upper 40 m.

Since shear modulus is the ratio of stress over strain and shear-wave velocity is a function of shear modulus and density, it is possible to estimate relative stress of overburden rocks (shear modulus) from shear-wave velocity values. Local increases in shear-wave velocity above background and without correlation to changes in lithology can be equated to increases in stress associated with changes in the distribution of overburden roof rock loading above solution jugs. Relative shear-wave velocity lows may be associated with remnants of a partial or incremental collapse whose vertical movement has been arrested by bulking, reduction in overburden stress due to changes in void geometry resulting in stress redistribution within roof rock, or changes in rock strength due to different geologic properties related to natural variation.

Overall, shear-wave velocity directly over or in proximity to most of the 47 wells in this year's study are consistent with natural geologic conditions and a normal stress regime as observed in previous years' studies. Results suggest the shale overburden across the site is currently in a state of relative stability with localized changes suggesting possible future stress redistribution (which could include vertical migration) at less than a dozen wells. Overburden materials at or near eight wells from this August 2024 survey were interpreted to have subtle but notable changes in overburden characteristics relative to past years or expected for native conditions. Bedrock velocity at wells 2A and 4B, a major focus of past reports due to dynamic overburden conditions and possible limited failure at depth, remains anisotropic and elevated

along line 10 suggesting dynamic changes continue in this area. Timelapse variability may suggest dynamic stress changes associated with changes in roof structures or characteristics of salt jugs have occurred near wells 52, 53, 14B, and 22A. Shear-wave velocity at these wells returned to native/expected in 2024, suggesting a current state of relative stability. Although a slightly increased depth of investigation between wells 87 and 88 could represent increased velocity in this area, it is likely an apparent increase caused by higher mode surface wave energy. Inversion was unstable on line 12 using several suitable passive sources, results in a velocity profile that is clearly rich in artifacts. Given the consistent velocity profiles observed at this line for most of the past decade, the risk of vertical migration is low and a mid-year survey is unnecessary prior to the next annual survey.

Introduction

Material properties (specifically stress accumulations) measured as a function of depth above abandoned salt jugs in Hutchinson, Kansas, appear related to the load density associated with the tensional dome of these jugs. Localized escalation in stress (as indicated by increased shear-wave velocity) above subterranean voids is one indicator of an increased potential for roof failure and void migration (Eberhart-Phillips et al., 1989; Dvorkin et al., 1996; Khaksar et al., 1999; Sayers, 2004). Previous studies, using both active and passive seismic wavefield characteristics, suggest perturbations in the shear-wave velocity field immediately above voids can be correlated to characteristics of the unsupported roof spans of salt jugs in the Hutchinson area (Sloan et al., 2010).

The strength of individual rock layers can be qualitatively described in terms of stiffness/ rigidity and empirically estimated from relative comparisons of shear-wave velocity measurements. Shear-wave velocity is directly proportional to stress and inversely related to non-elastic strain. Since the shear-wave velocity of earth materials changes when stress and any associated elastic strain on those materials becomes "large," it is reasonable to suggest load-bearing roof rock above mines or dissolution voids may experience elevated shear-wave velocities due to loading between pillars or, in the case of voids, loading between supporting side walls. This localized increase in shear velocity is not related to increased strength but to increased load as defined by Young's Modulus. High-velocity shear-wave encompassing low-velocity anomalies ("halo" anomalies) are suggested to be key indicators of near-term roof failure. All these phenomena have been observed within the overburden above voids in the Hutchinson Salt Member in Hutchinson at depths greater than 30 m below the bedrock surface.

Previous research projects at the Carey Boulevard Research Area (CBRA) correlated measured shear-wave velocities with the condition of dissolution void roofs and the physical properties of the overburden at selected locations on Vigindustries legacy solution mining property in Hutchinson. In 2008, active seismic reflection was used to evaluate the effectiveness of shear-wave velocity as a relative measure of local stress above voids representative (in the size and depth) of those prevalent at the Vigindustries site (Miller et al., 2009). It was determined that the integrity of the overlying strata could be reasonably estimated using shear-wave seismic reflection imaging. The lack of necessary ultra-low-frequency surface waves in the recorded wavefield negated attempts to use active-source multi-channel analysis of surface waves (MASW) to estimate shear velocity in the lithified rocks above the voids and near the top of bedrock (Miller et al., 2009).

Uncontrolled local industrial and transportation activities represent sound sources that can produce the necessary low frequency seismic waves to interrogated rock material at depth

greater than 60 m using passive methods (Miller, 2011). Key to this method is the ability to estimate shear-wave velocities using MASW to depths more than double those possible using standard active sources (Park et al., 2004). Results of passive MASW studies at and near this site suggest that this method is effective in identifying jugs with heightened risk for upward migration (Miller, 2011; Ivanov et al., 2013).

Following the active seismic imaging study in 2008, two-dimensional (2-D) passive MASW surveys have been acquired at the Vigindustries site since 2012 to appraise the stability/consistency of overburden at selected wells (Table 1). Results of these investigations suggested a normal stress regime with natural geologic variation above most wells. Shear velocity above a few wells was noted to be outside what might be considered normal for the area and justified more attention. Individually, each profile represents a snapshot in time. When combined with previous observations at the same locations, timelapse analysis can be used to monitor for temporal variation in shear velocity, providing insight into relative stability and void dynamics.

Table 1. Dates of wells evaluated during 2-D passive MASW surveys at the CBRA.

Date	Wells
August 2012	2A, 1B, 2B, 3B, 5B, 6B, 7B, 12B
October 2012	2B, 4B, 6B, 17, 45, 52, 53, 59
March 2013	2A, 4B
November 2014	2A, 3B, 4B
March 2015	1B, 2B, 3B, 6B, 8A, 8B, 10B, 11B, 12B, 13B, 14B, 15B, 17, 18, 22A, 23, 23B, 29, 30, 39, 41, 42, 44, 45, 46, 86, 87, 88, 89, 90, 92
May 2015	2A, 4B
June 2015	4A, 6B, 7A, 7B, 52, 53, 59, 60
November 2017	2A, 4A, 7A, 8A, 1B, 2B, 3B, 4B, 6B, 7B, 8B, 10B, 11B, 12B, 13B, 14B, 15B, 17, 18, 22A, 23, 23B, 29, 30, 39, 41, 42, 44, 45, 46, 52, 53, 59, 60, 86, 87, 88, 89, 90, 92
October 2018	2A, 4B
December 2018	1B, 2B, 3B, 4A, 4B, 6B, 7A, 7B, 8A, 8B, 10B, 11B, 12B, 13B, 14B, 15B, 17, 18, 22A, 23B, 23, 29, 30, 39, 41, 42, 44, 45, 46, 52, 53, 59, 60, 86, 87, 88, 89, 90
December 2019	1B, 2A, 2B, 3B, 4A, 4B, 5B, 6B, 7A, 7B, 8A, 8B, 10B, 11B, 12B, 13B, 14B, 15B, 17, 18, 22A, 23B, 23, 29, 30, 39, 42, 44, 45, 46, 52, 53, 59, 60, 88, 89, 90, 92
August 2020	2A, 4A, 7A, 15B, 59
November 2020	1B, 2A, 2B, 3B, 4A, 4B, 5B, 6B, 7A, 7B, 8A, 8B, 10B, 11B, 12B, 13B, 14B, 15B, 17, 18, 22A, 23B, 23, 29, 30, 39, 42, 44, 45, 46, 52, 53, 59, 60, 88, 89, 90, 92
November 2021	1B, 2A, 2B, 3B, 4A, 4B, 5B, 6B, 7A, 7B, 8A, 8B, 10B, 11B, 12B, 13B, 14B, 15B, 17, 18, 19, 20, 22A, 23B, 23, 25, 26, 29, 30, 33, 36, 39, 41, 42, 44, 45, 46, 52, 53, 59, 60, 88, 89, 90, 92, 94
March 2023	1B, 2A, 2B, 3B, 4A, 4B, 5B, 6B, 7A, 7B, 8A, 8B, 10B, 11B, 12B, 13B, 14B, 15B, 17, 18, 19, 20, 22A, 23B, 23, 25, 26, 29, 30, 33, 36, 39, 41, 42, 44, 45, 46, 52, 53, 59, 60, 88, 89, 90, 92, 94
November 2023	2A, 4B
August 2024	1B, 2A, 2B, 3B, 4A, 4B, 5B, 6B, 7A, 7B, 8A, 8B, 10B, 11B, 12B, 13B, 14B, 15B, 17, 18, 19, 20, 22A, 23B, 23, 25, 26, 29, 30, 33, 36, 39, 41, 42, 44, 45, 46, 52, 53, 59, 60, 87, 88, 89, 90, 92, 94

Geologic and Geophysical Setting

The Permian-aged Hutchinson Salt Member occurs in central Kansas, northwestern Oklahoma, and the northeastern portion of the Texas panhandle and is prone to and has an extensive history of dissolution and formation of sinkholes (Figure 1). In Kansas, the Hutchinson Salt Member possesses an average net thickness of 75 m and reaches a maximum of more than 150 m in the southern part of the basin. Deposition occurring during fluctuating sea levels caused numerous halite beds, 0.2 to 3 m thick, to be formed interbedded with shale, minor anhydrite, and dolomite/magnesite. Individual salt beds may be continuous for only a few miles despite the remarkable lateral continuity of the salt as a whole (Walters, 1978).

The distribution and stratigraphy of the salt is well documented (Dellwig, 1963; Holdoway, 1978; Kulstad, 1959; Merriam, 1963). The salt reaches a maximum thickness in central Oklahoma and thins to depositional edges on the north and west, erosional subcrop on the east, and facies changes on the south. The increasing thickness toward the center of the salt bed is due to a combination of increased salt and more and thicker interbedded anhydrites. The Stone Corral Formation (a well-documented seismic marker bed) overlies the salt throughout Kansas (McGuire and Miller, 1989). Directly above the salt at this site is a thick sequence of Permian shale overlain by a saturated interval of Plio-Pliestocene sediments.

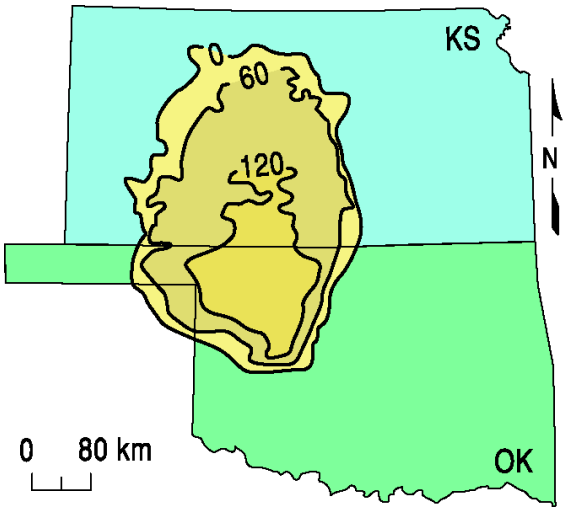

Figure 1. Approximate extent of salt formation, with contour intervals expressed in meters.

The upper 760 m of rock at this site is Permian shale (Merriam, 1963). The lower Wellington Shale (top at ~225 m deep), Hutchinson Salt (top at ~120 m deep), upper Wellington Shale (top at ~70 m deep), and Ninnescah Shale (top at ~15 m deep) make up the Permian portion of the section (Figure 2). Bedrock is defined as the top of the Ninnescah Shale with the unconsolidated Pliocene-Pleistocene Equus beds making up the majority of the upper 15 m of sediment. The thickness of Quaternary alluvium that fills the stream valleys and paleosubsidence features goes from 0 to as much as 90 m, depending on the dimensions of the features.

Recent dissolution of the salt and resulting subsidence of overlying sediments forming sinkholes has generally been associated with mining or saltwater disposal (Walters, 1978). Historically, these sinkholes can manifest themselves as a risk to surface infrastructure. The rate of surface subsidence can range from gradual to very rapid. Besides risks to surface structures, subsidence features potentially jeopardize the natural segregation of groundwater aquifers, greatly increasing their potential to negatively impact the environment (Whittemore, 1989, 1990). Natural sinkholes resulting from dissolution of the salt by localized leaching within natural flow systems that have been altered by structural features (such as faults and fractures) are not uncommon west of the main dissolution edge (Merriam and Mann, 1957).

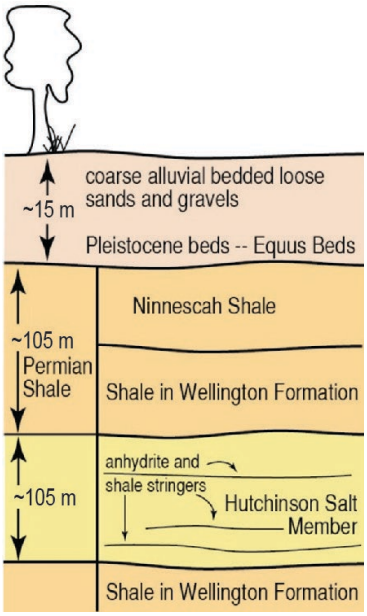

Figure 2. Generalized geology.

Caprock and its characteristics are a very important component of any discussion concerning dissolution, subsidence, and formation of sinkholes. The Permian shales (Wellington and Ninnescah) that overlie the Hutchinson Salt Member are highly variable and can range from less than 60 m to more than 100 m thick in this area and are characterized as generally unstable when exposed to freshwater, being susceptible to sloughing and collapse (Swineford, 1955). These Permian shales tend to be red or reddish-brown and are commonly referred to as "red beds." Permian red beds are extremely impermeable to water and have provided an excellent seal between the freshwaters of the Equus beds and the extremely water-soluble Hutchinson Salt Member. The modern-day expanse and mere presence of the Hutchinson Salt is due to the protection from freshwater provided by these red beds.

Isolating the basal contact of the upper Wellington Formation provides key insights into the general strength of roof rock expected, if dissolution-mined salt jugs reach the top of the salt zone. Directly above the salt/shale contact is approximately 6 m thick dark-colored shale with joint and bedding cracks filled with red halite (Walters, 1978). Once unsaturated brine comes in contact with this shale layer, these red halite-filled joints and bedding planes are rapidly leached, leaving an extremely structurally weak layer.

Field Layout and Data Acquisition

To ensure the highest quality (e.g., signal-to-noise ratio, S/N) data and maximum crew safety, receivers were deployed during daylight hours and train data were recorded at night when cultural and industrial noise was minimal, thereby providing the highest possible S/N. Analysis

of previous seismic energy sources captured during passive recording at this site clearly indicated trains at distances of 2 kilometers (km) or more provided the best broad spectrum, low-frequency seismic energy (Miller, 2011). Since seismic energy with characteristics best suited for this study may arrive when trains are at distances greater than can be detected by spotters, seismic energy was recorded continuously throughout the night to capture of all times, ensuring optimum data.

Data were acquired August 12-15, 2024. A total of thirteen seismic lines (Figure 3) were deployed during the day over this four-day period. Line layout was designed to cross directly over wells of interest. A 2-D square grid of receivers was recorded simultaneously to allow determination of the incident orientation of passive seismic energy. Seismic receivers were single ION 4.5 Hz geophones spaced at 3 m intervals. The westernmost 5 geophones on line 10 were located on the road used to access the grain elevator, requiring rock plates instead of steel spikes. The seismic lines collectively totaled approximately 5000 m in length. The 2-D monitoring/alignment grid consisted of 128 receivers spaced at 5 m intervals and was configured to form four concentric expanding squares with 10, 30, 50, and 70 m sides (Figure 4). Data were recorded with a 400+ channel 24-bit Geometrics Geode distributed seismic system. Line 15 and the 2-D grid utilized a wireless nodal acquisition system by GTI that recorded output from the geophones. Seismic records from the Geometrics system were 30 seconds (s) long with a 2 millisecond (ms) sampling interval. In total, 3558 seismic records were recorded.

Processing and Analysis

Data were processed using algorithms developed at the Kansas Geological Survey (KGS). The passive method used for this study is well published and has consistently proven effective producing good-quality results on other studies (Park et al., 2004; Ivanov et al., 2013). The continuous-data-acquisition method records energy from nearby sources at various orientations with respect to the seismic line. Data from the 2-D grid are evaluated for optimized source alignment with respect to each 1-D seismic line allowing data rotation and analysis or direct analysis of only data from near in-line sources.

For each line, the surface-wave amplitudes recorded by the 2-D grid were plotted as phase velocity versus frequency across a range of azimuths (0 to 360 degrees) (Figure 5), relative to the seismic line. This display was effective for identifying the best broad-band, low-frequency source energy with an azimuth as near zero as possible. Seismograms for each line were selected and segmented into the shortest groups of receivers ("spread length") with optimum source characteristics that resulted in dispersion patterns on phase velocity versus frequency plots with the greatest percentage of high-amplitude fundamental-mode Rayleigh-wave energy and minimal higher-order surface-wave interference (Figure 6).

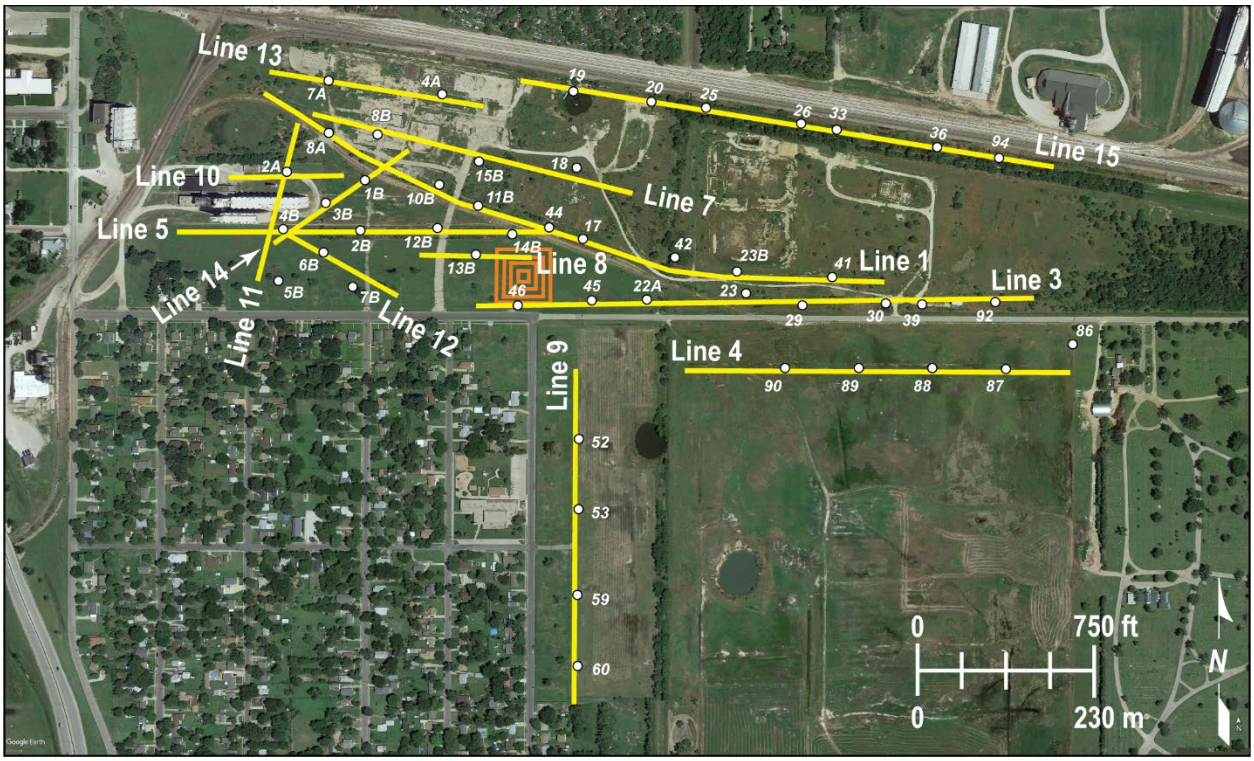

Figure 3. Aerial photo with GPS locations of thirteen seismic lines, 2-D grid of receivers (orange squares), and wells in the November 2021 study.

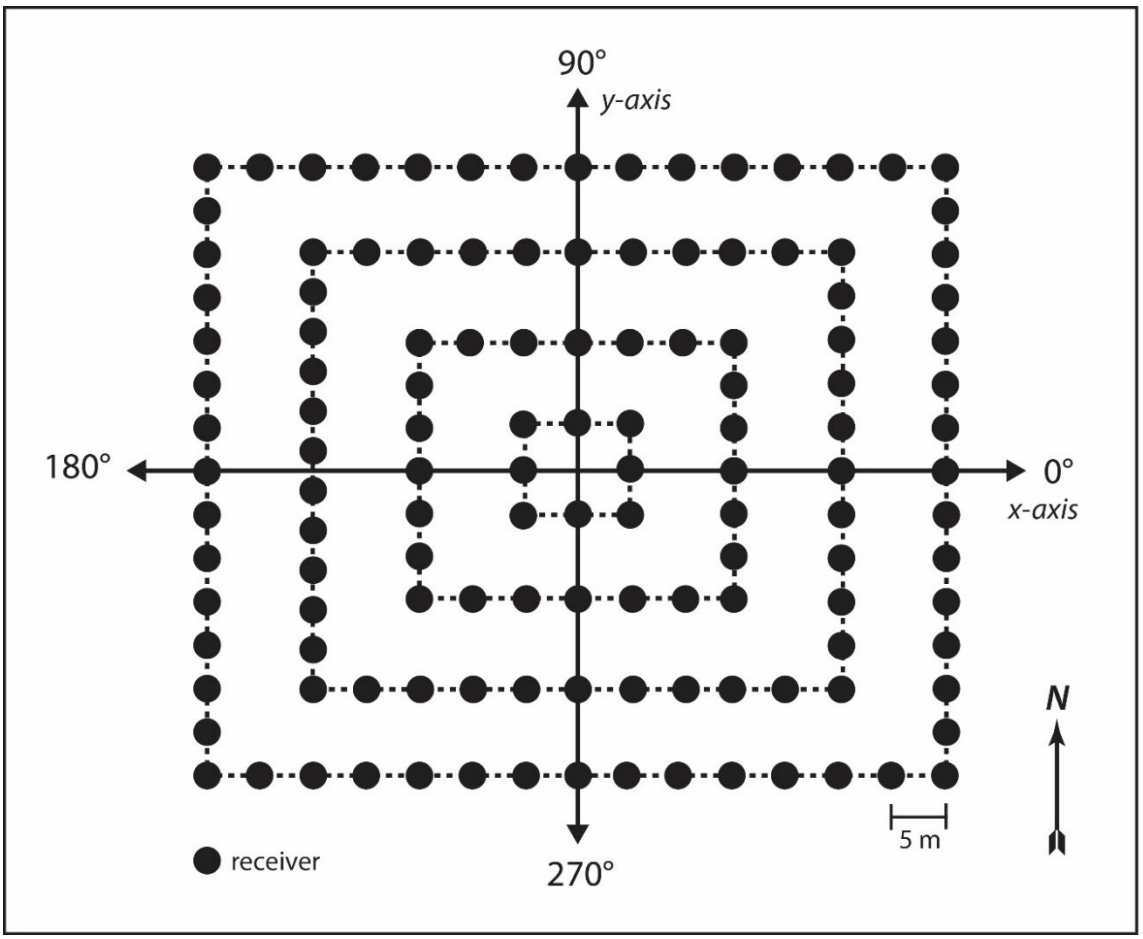

Figure 4. Four nested square arrays were deployed each night to construct the 2-D square grid for determining incident source azimuth information.

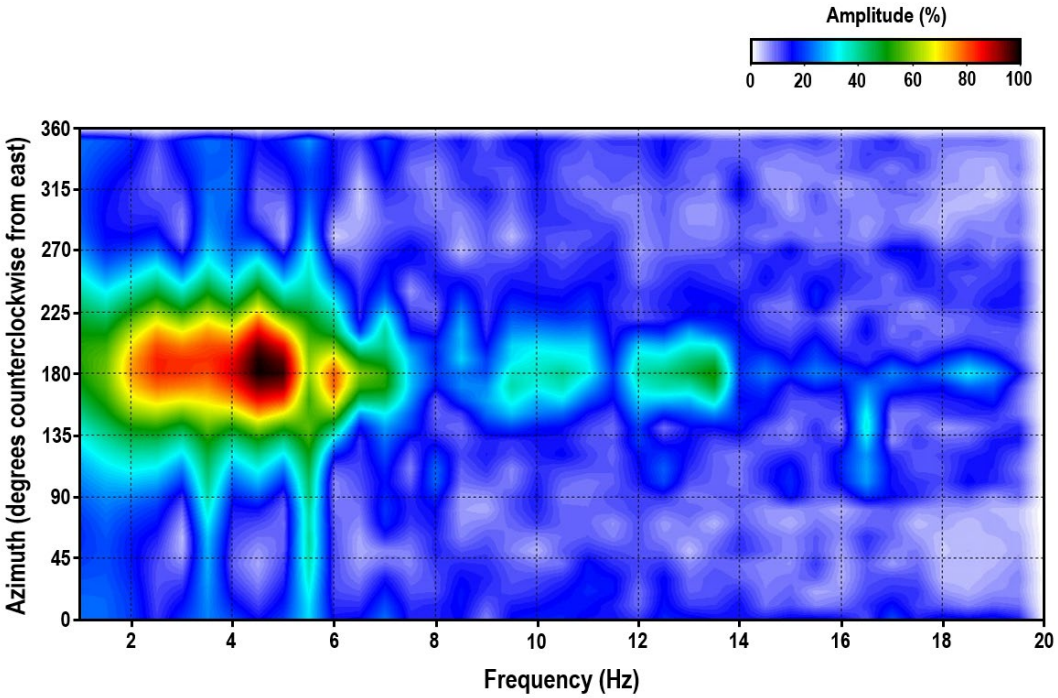

Figure 5. Azimuth plot indicating the direction of the dominant passive source energy (in degrees counter-clockwise from east). Here, the dominant passive source energy is centered on approximately 180°.

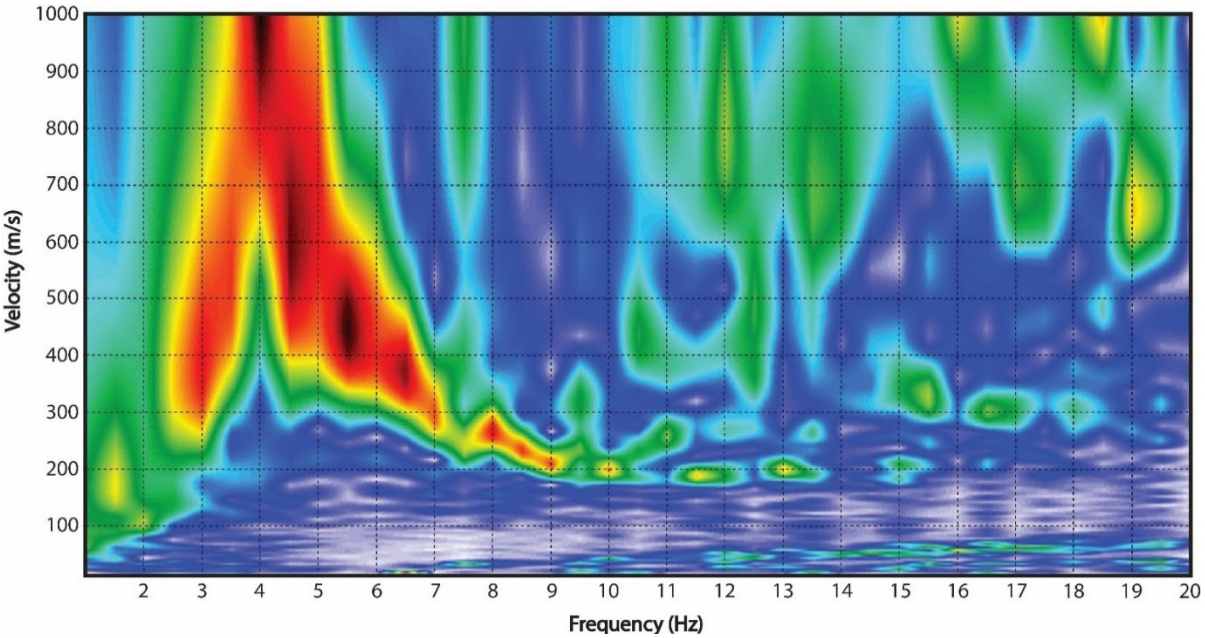

Figure 6. Dispersion pattern with high signal-to-noise ratio of the fundamental-mode Rayleigh wave.

Fundamental mode dispersion curves were picked and inverted to obtain a 2-D section of shear-wave velocity as a function of depth. The apparent velocity (v_{app}) is:

$$v_{app} = \frac{v_{act}}{(\cos\theta)} \quad (1)$$

where v_{act} is the actual seismic velocity and θ is the azimuth of the source with respect to the seismic line determined from the azimuth versus frequency plot. Thus, the percent increase in velocity (Δv) is:

$$\Delta v = \frac{1}{\cos\theta} - 1 \quad (2)$$

Equation 2 was used to calculate the increase in velocity due to the source azimuth for each line (Table 2).

Table 2. Directions of the passive seismic sources and the seismic lines; spread length used for processing, the angle of the source with respect to the line (θ, in degrees counterclockwise from east), and the percent increase in apparent velocity (Δv) attributable to oblique source orientations.

	processing spread length(s)	source orientation	line orientation	θ	Δv
Line 1	90 m 99 m	150° 0°	135° 180°	15° 180°	3.53% 0%
Line 3	99 m	180°	180°	0°	0%
Line 4	81 m	200°	180°	20°	7.0%
Line 5	99 m	180°	180°	0°	0%
Line 7	99 m	155°	165°	10°	1.52%
Line 8	72 m	180°	180°	0°	0%
Line 9	99 m	270°	86°	184°	0.24%
Line 10	81 m	180°	180°	0°	0%
Line 11	72 m	45°	74°	29°	13.5%
Line 12	81 m	150°	152°	2°	0.06%
Line 13	81 m	160°	172°	12°	2.23%
Line 14	81 m	45°	35°	10°	1.52%
Line 15	81 m	160°	165°	10°	1.52%

Field Results and Observations

General Trends

The average velocity of the upper 15 m is approximately 175 m/s, consistent with the unconsolidated/alluvial sediment in this area and downhole data acquired in well 15B in January 2023. The velocity gradient at 15 m coincides with the interface between the unconsolidated sediment and shale bedrock. Average depth of investigation was 50-60 m across all lines as a result of surface wave frequencies generally above 4 Hz—lower frequencies would have resulted in deeper sampling depths. Dispersion curves were obtained using varying spread lengths for each line, selected to avoid distortion in surface wave dispersion patterns at low frequencies. Using the shortest optimal spread length on each line resulted in high lateral resolution and the largest spatial extend of the resulting 2-D profiles while maintaining dispersion patterns at lower frequencies.

Line 1

Line 1 (Figure 7) is a slightly curved NW-E oriented line that extends across wells 8A, 10B, 11B, 44, 17, 42, 23B, and 41 (Table 3). This is the only line with nonlinear receiver alignment. Two different source files were used to process the line, one with an azimuth of 120 degrees and the other 180 degrees. The maximum depth of investigation was between 45 and 55 m, which is similar to the 2023 survey. Identical spread lengths were used in 2023 and 2024, resulting in the same spatial area covered.

Table 3. Wells and corresponding station numbers across line 1.

Well	8A	10B	11B	44	17	42	23B	41
Station No.	1033	1086	1105	1136.5	1152.5	1196	1223.5	1265

Overall, the bulk-velocity trend observed in August 2024 is generally consistent with the past three years' results. A halo anomaly at well 8A observed in 2020 (dashed circle in Figure 7a) persisted relatively unchanged in 2021 and 2023 (Figure 7c). The velocity at well 8A is more consistent with adjacent areas in 2024. Overall, the velocity variation across line 1 is minimal and all identified anomalies are within the bounds of native material properties.

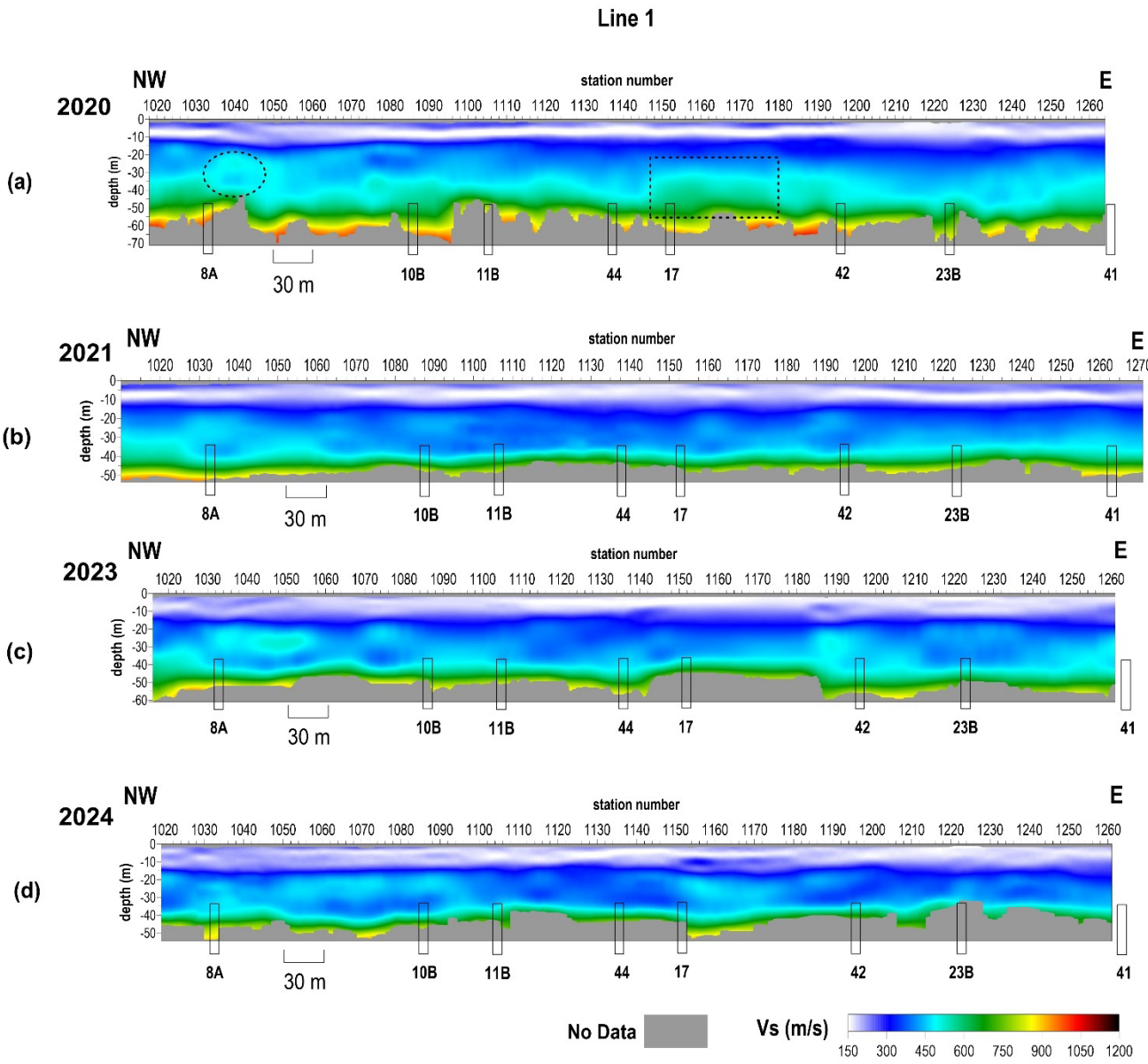

Figure 7. Shear wave velocity profiles from line 1 from (a) November 2020, (b) November 2021, (c) March 2023, and (d) August 2024.

Line 3

Line 3 (Figure 8) is oriented W-E and extends over wells 46, 45, 22A, 23, 29, 30, 39, and 92 (Table 4). A window splitting algorithm was used to improve the signal along this line. The general bulk velocity profile remains consistent with past studies, with velocity trends similar to the 2021 survey (Figure 8b). A subtle increase in velocity was observed near well 22A extending westward toward well 45 in 2020 and 2023. The velocity profile at well 22A in 2024 is consistent with 2021 (native conditions). The velocity profiles near well 92 (stations 3215-3240) are somewhat variable from year to year and may be associated with redistribution of stress in the overburden due to localized failure. Overall, 2024 results are similar to 2021 and within the range expected for native bedrock.

Table 4. Wells and corresponding station numbers across line 3.

Well	46	45	22A	23	29	30	39	92
Station No.	3025	3057	3080.5	3124	3148	3183.5	3199	3230.5

Line 4

Line 4 is a W-E oriented line that crosses wells 90, 89, 88, and 87 at stations 4044, 4076, 4107.5, and 4139.5, respectively (Figure 9). A slightly shorter spread length used in 2024 increased spatial coverage, extending the velocity profile directly over well 87. Due to degradation of signal on the east end of the line, a second passive source was used on this portion of the line and results were stitched into a single profile at station 4118. The velocity profile on line 4 is mostly consistent with location determined to have native conditions. There appears to be an area of slightly elevated velocity and/or increased depth of investigation between wells 88 and 87, consistent in results from both sources. **Although this is likely local variation in surface wave propagation, it warrants awareness and reassessment during the next annual passive survey**.

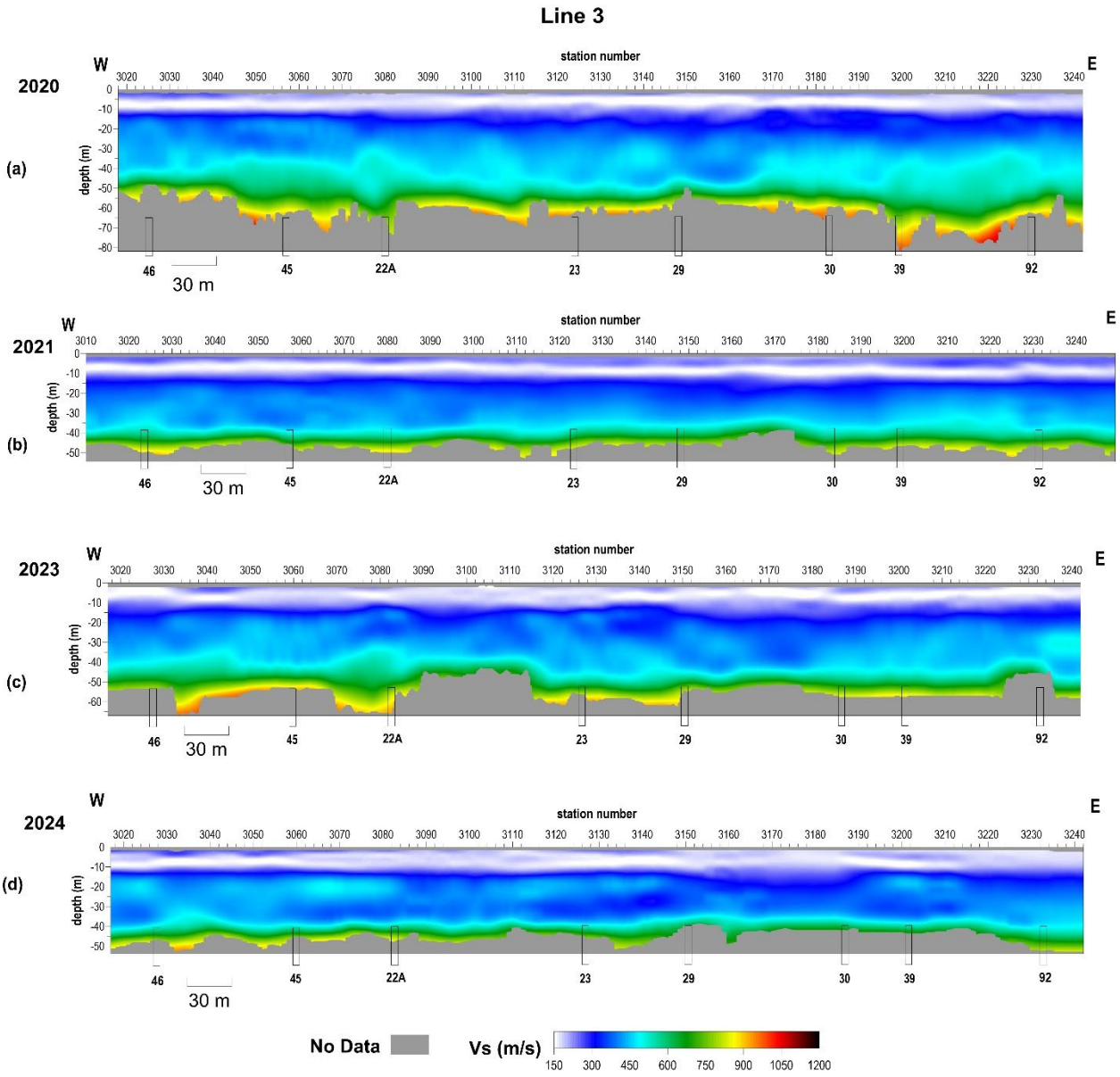

Figure 8. Shear-wave velocity profiles from line 3 from (a) November 2020, (b) November 2021, (c) March 2023, and (d) August 2024.

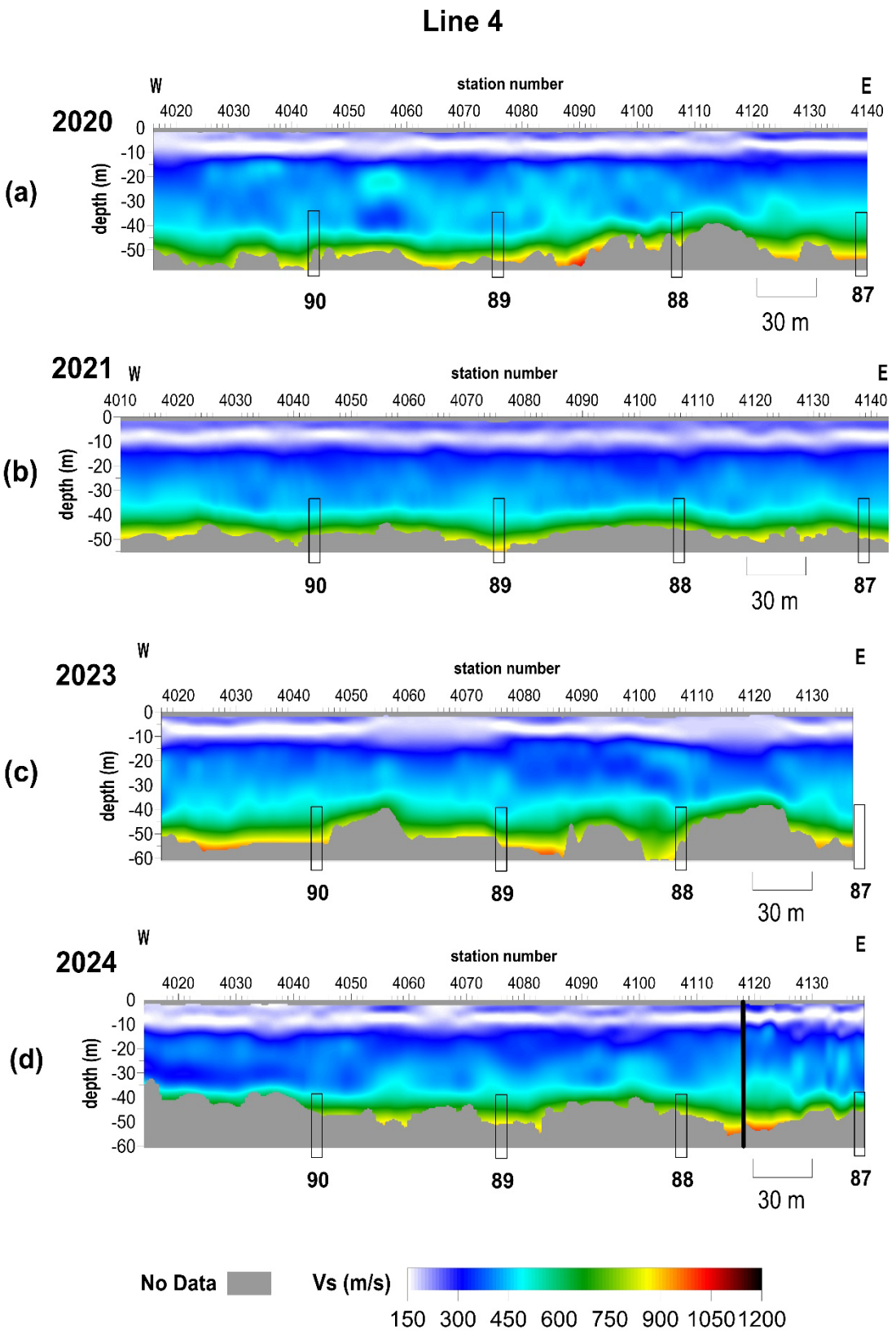

Figure 9. Shear-wave velocity profiles from line 4 from (a) November 2020, (b) November 2021, (c) March 2023, and (d) August 2024.

Line 5

Line 5 is oriented W-E and crosses wells 4B, 2B, 12B, and 14B at stations 5027.5, 5061, 5094, and 5126.5, respectively (Figure 10). Subtle anomalous velocity trends have consistently been observed near well 14B in previous years, possibly suggesting dynamic conditions below the imaging depths. Overall, the velocity profile on this line is consistent with native conditions in 2024. Minor variability is likely related to source characteristics and uncertainty inherent to the MASW method.

Line 7

Line 7 is oriented NW-SE and crosses over wells 8B, 15B, and 18 approximately located at stations 7028, 7073, and 7114, respectively (Figure 11). Well 15B has a history of dynamic shear-wave velocity and depth of investigation (see Figure A-1 in the appendix). An area of elevated velocity at depth centered on well 15B was observed in 2015. Velocity decreased in 2017 and again in 2018, returning to velocities expected for normal conditions/stress. Velocity profiles in 2020 were somewhat anomalous but returned to normal conditions consistent with the rest of line 7 in 2021. In the present study, overall bulk velocity remains relatively consistent across the line compared to previous studies and is consistent with the native material. The depth of investigation is similar to 2023 with reduced uncertainty/error throughout the line. The dome-shaped area of elevated velocity west of well 18 in 2023 (Figure 11c) is not present in 2024. This area had uncertainty in the dispersion curves due to higher mode interference in 2023, which likely caused the apparent velocity increase.

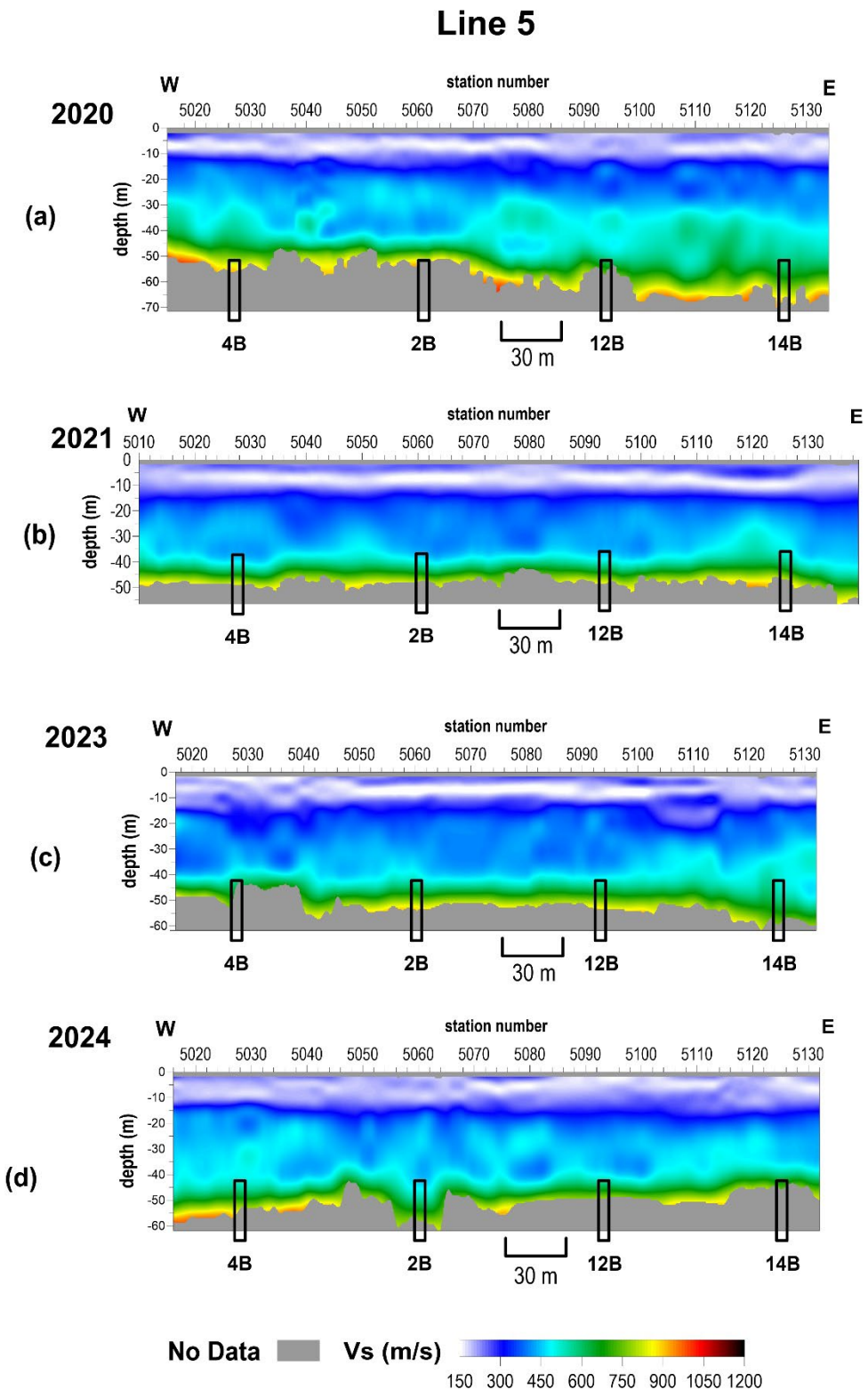

Figure 10. Shear-wave velocity profiles from line 5 from (a) November 2020, (b) November 2021, (c) March 2023, and (d) August 2024.

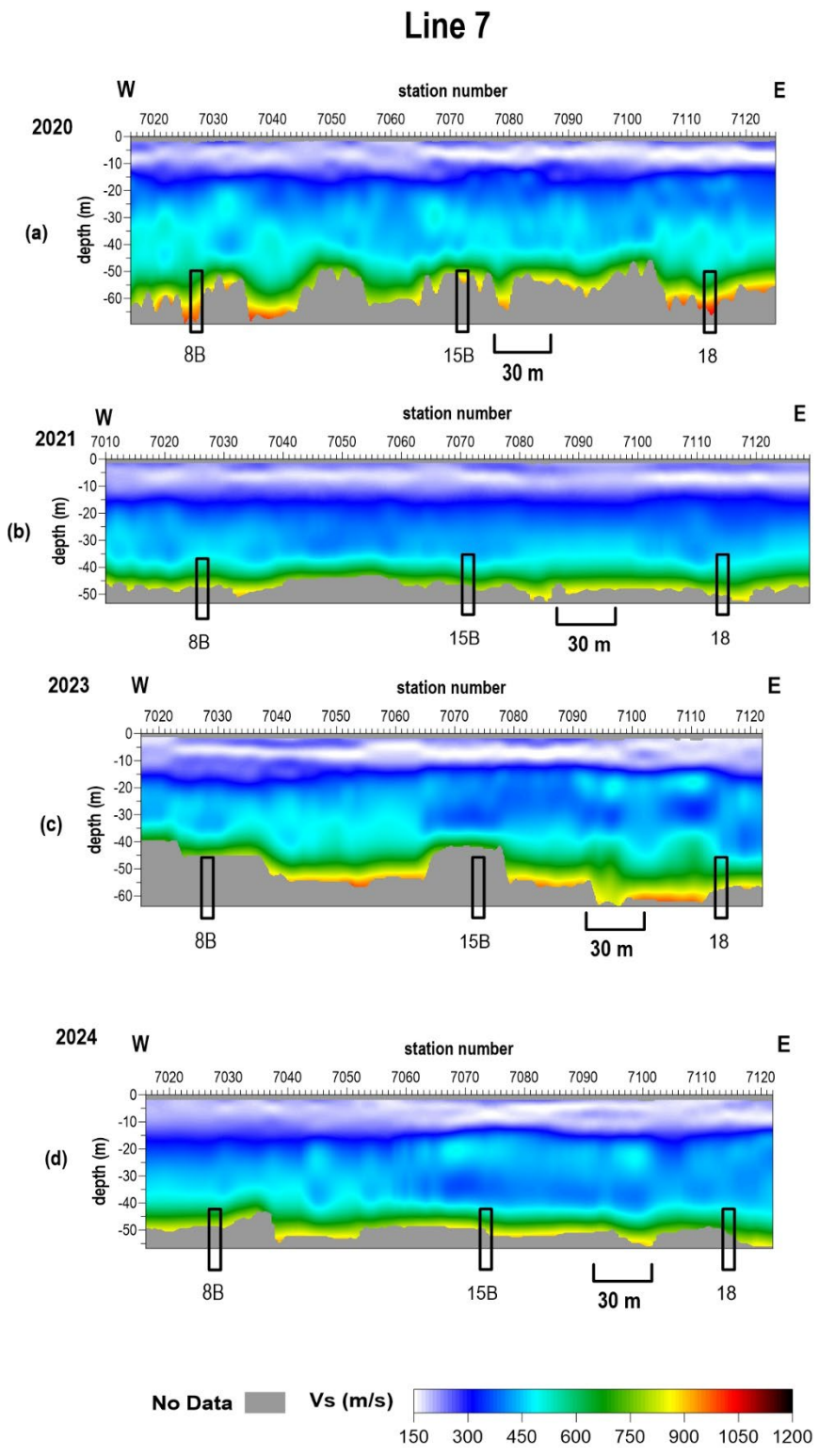

Figure 81. Shear-wave velocity profiles from line 7 from (a) November 2020, (b) November 2021, (c) March 2023, and (d) August 2024.

Line 8

Line 8 is oriented W-E and intersects well 13B at station 8025 (Figure 12). Four westernmost stations on line 8 extend across the paved entry road at the CBRA; these four stations (8008-8011) required rock plates rather than steel spikes to couple sensors to the ground surface. The bulk velocity profile in 2024 is consistent with previous year's results. Somewhat dynamic velocities have been observed at well 13B in the past few years. Velocity was elevated in 2018 and returned to normal stress conditions representative of native areas in 2019. A minor velocity inversion was observed in 2020, and stress conditions have again returned to levels considered normal since 2021. These timelapse observations may reflect periodic stress build up, roof failure, and associated drops in stress.

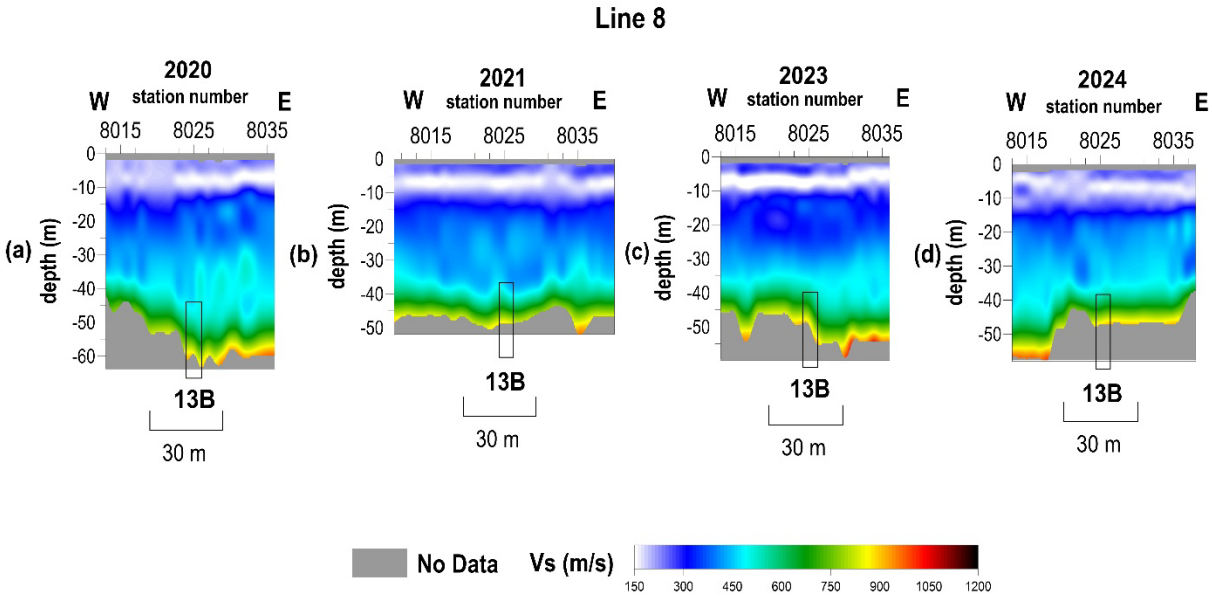

Figure 92. Shear-wave velocity profiles from line 8 from (a) November 2020, (b) November 2021, (c) March 2023, and (d) August 2024.

Line 9

Line 9 is a N-S oriented line that runs parallel to Williams Street and crosses wells 52, 53, 59, and 60 at stations 9031, 9061, 9098, and 9127, respectively (Figure 13). Slight variability and undulation at depth is likely a result of uncertainty due to interference from a higher mode or offline source energy.

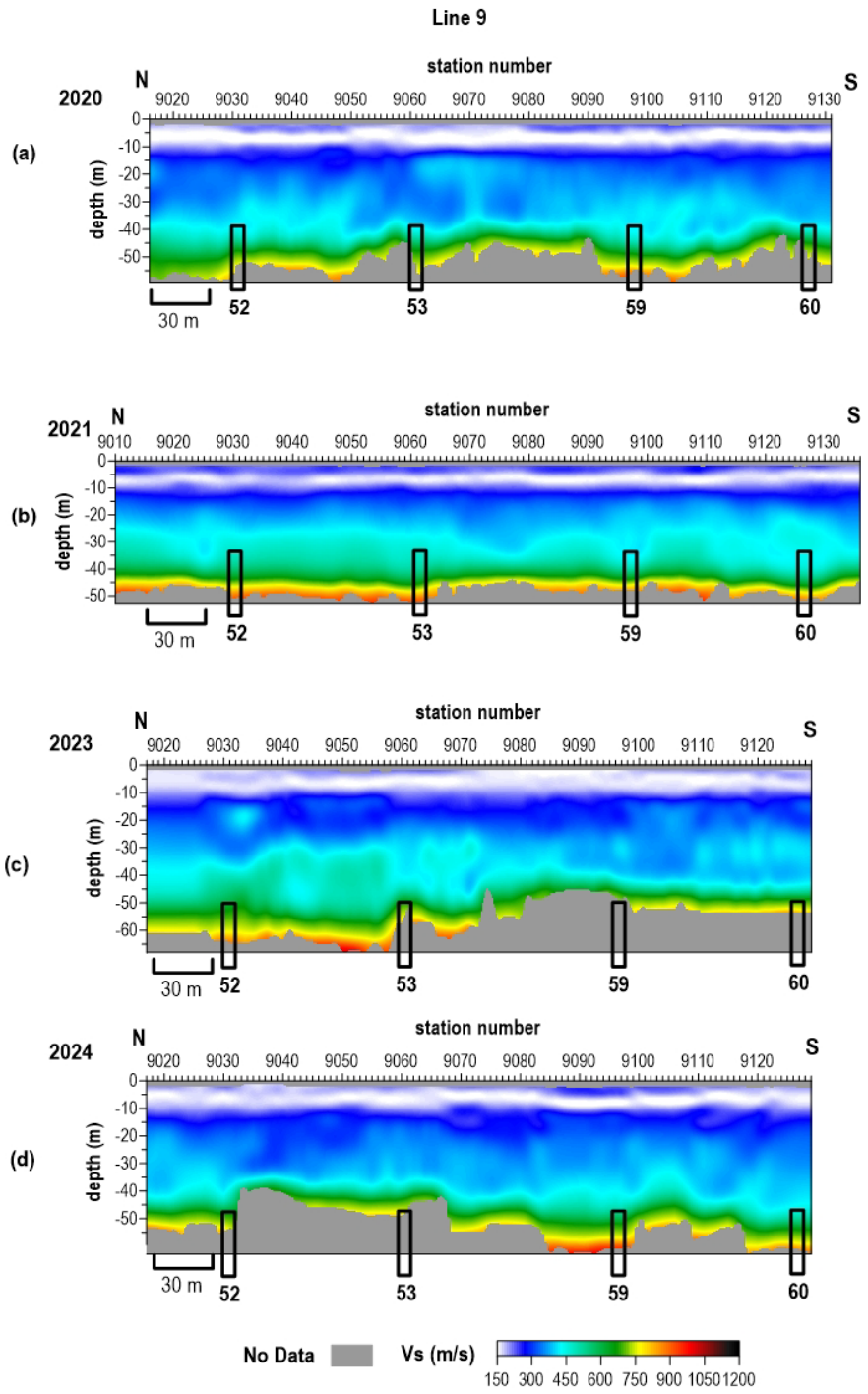

Figure 103. Shear-wave velocity profiles from line 9 from (a) November 2020, (b) November 2021, (c) March 2023, and (d) August 2024.

Line 10

Line 10 is a W-E oriented line that crosses well 2A at station 1022.5 (Figure 14). Timelapse changes observed at well 2A since 2013 suggest periods of elevated stress/velocity, subsequent roof rock failure and reduced overburden strength, and periods of relative stability (see Figure A-2 in the appendix). Between the May 2015 and November 2017 surveys, velocity in the overburden at well 2A increased slightly (~15%) and was consistent with native bedrock velocity. This suggests the void at that time was in a state of relative stability with only gradual changes in stress. Multiple mode behavior was noted west of well 2A in 2020 suggesting heterogeneity at deeper depths where multiple stress states may have existed within the shale bedrock, and a period of relative stability in 2021. Velocity was slightly elevated in 2023 and in 2024 increased 30% or more relative to velocity expected for native conditions. The increased depth of investigation this year could be an effect of elevated velocity at depth. This suggests increased stress that will likely result in a spall event and subsequent redistribution of stress.

Line 11

Line 11 is oriented N-S over well 2A at station 1124 and well 4B at station 1151 (Figure 15). The average velocity below 30 m decreased 15% across line 11 from 2019 to 2020. Because such a corresponding decrease was not observed on the nearly perpendicular line 10, the velocity variation observed in 2020 was azimuthal and therefore anisotropic, which may be associated with changes in material strength associated with fractures. In 2023 and 2024, velocities are similar to 2020, possibly suggesting azimuthal anisotropy and changes in material strength influenced by fracture orientation. This anisotropy is particularly apparent in 2024, given the relatively large increase in velocity on line 10.

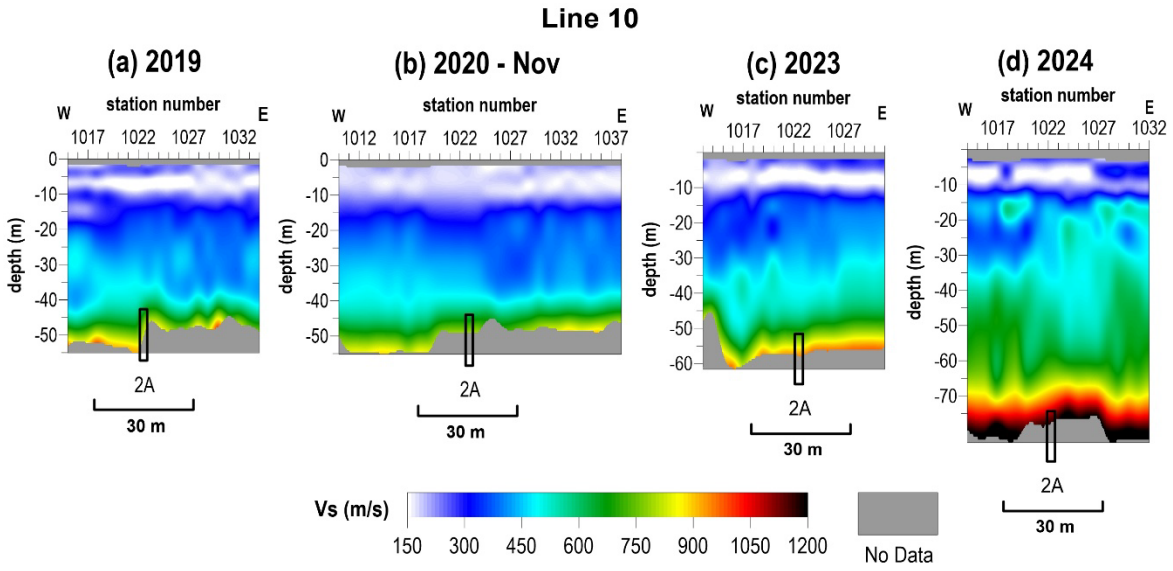

Figure 14. Shear-wave velocity profiles from line 10 from (a) November 2020, (b) November 2021, (c) March 2023, and (d) August 2024.

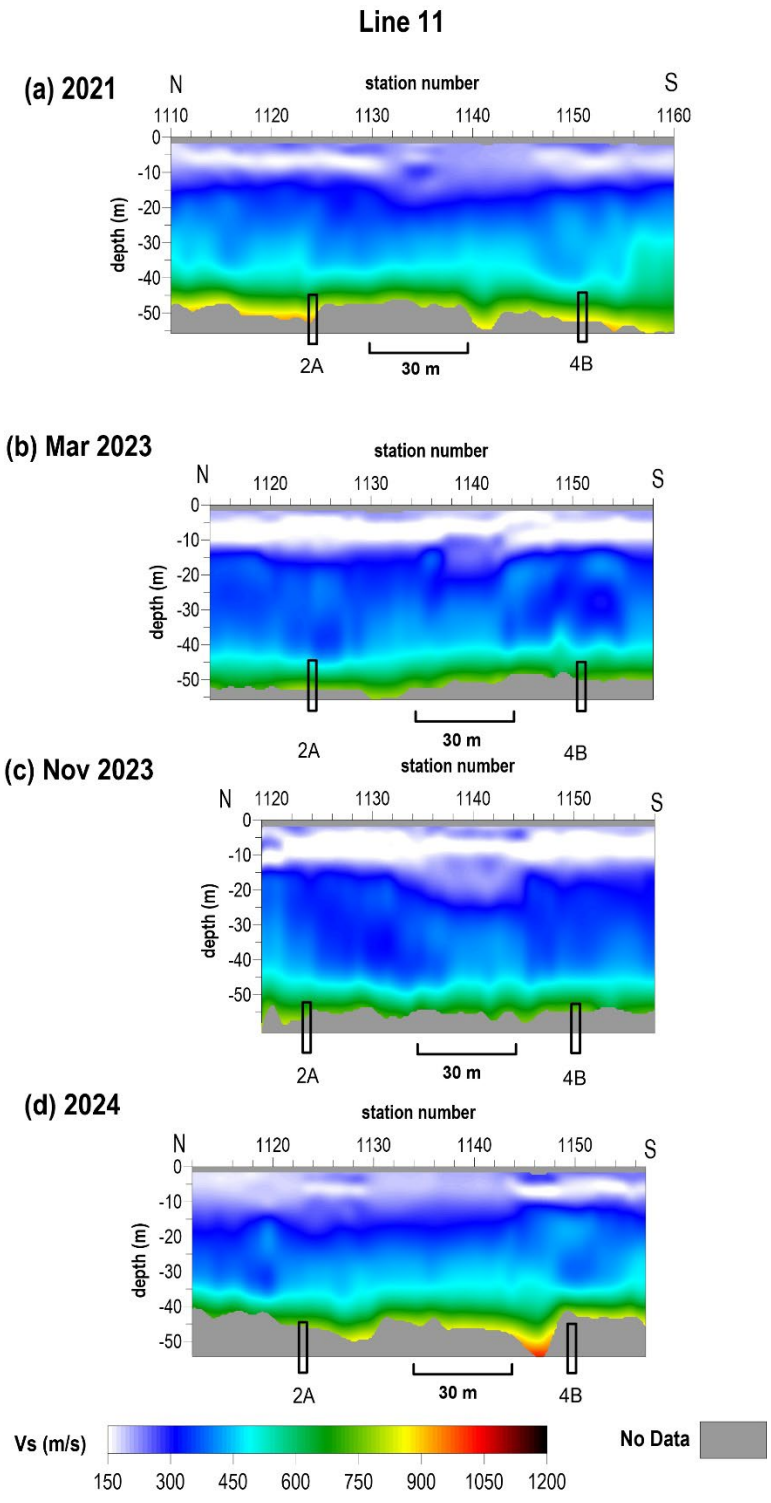

Figure 15. Shear-wave velocity profiles from line 11 from (a) November 2020, (b) November 2021, (c) March 2023, and (d) August 2024 investigation with approximate locations of well 2A and well 4B.

Line 12

Line 12 is a W-E oriented line that crosses wells 6B and 7B at stations 1238 and 1219, respectively (Figure 16). An approximately 25% velocity increase was observed in 2020 compared to previous years but was still within the range of bedrock velocity estimates on other lines at the CBRA and may have been a result of higher mode interference with the fundamental mode. Bulk velocities in 2021 returned to normal and are similar in 2023 but with a subtle dome-shaped area of elevated velocity in proximity to well 7B. These velocities are still within the expected range for bedrock at this site but may suggest gradually elevating velocity and possibly the start of increasing stress at 7B. It is possible the apparent velocity is higher due to uncertainty in dispersion curve picks from reduced S/N at corresponding frequencies. The 2024 passive sources were all very challenging to pick due to interference of higher mode or off-line energy, despite processing designed to enhance fundamental mode signal. Because of inversion instability, this year's results are artifact-rich and uninterpretable. Given the relative stability of velocities the past few years, it is likely not a cause for concern at this time.

Line 13

Line 13 is oriented W-E and intersects wells 7A and 4A located approximately at stations 1328 and 1376.5, respectively (Figure 17). The bulk velocity trend has remained relatively consistent since 2018. Velocities from 2024 appear to be very similar to 2021 with similar depths. Velocity values across this area are within normal range for native material and represent a normal stress regime. An apparent increase in velocity between 7A and 4A in 2023 was interpreted as a result of uncertainty. Return to native velocities in 2024 supports this interpretation and conditions on this line appear to be stable.

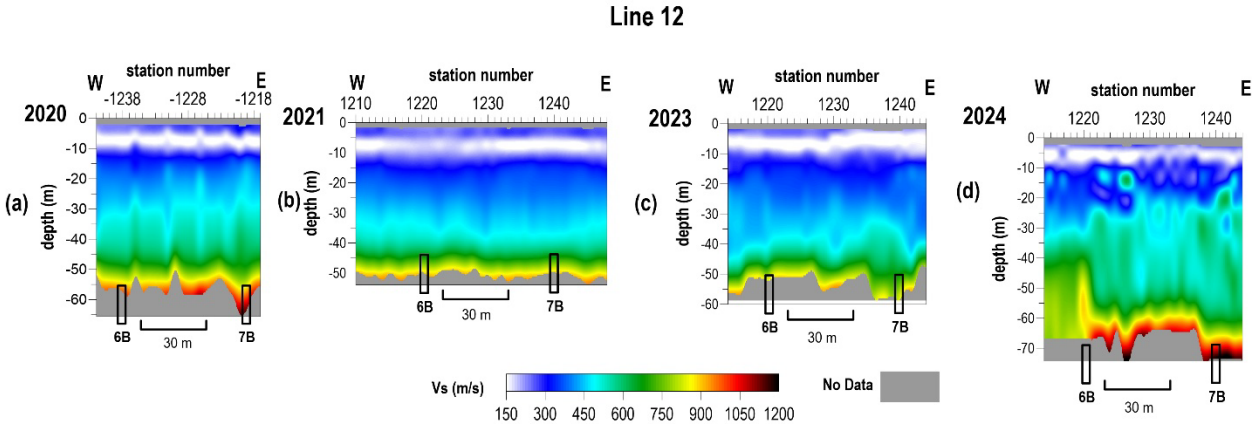

Figure 16. Shear-wave velocity profiles from line 12 from (a) November 2020, (b) November 2021, (c) March 2023, and (d) August 2024 investigation.

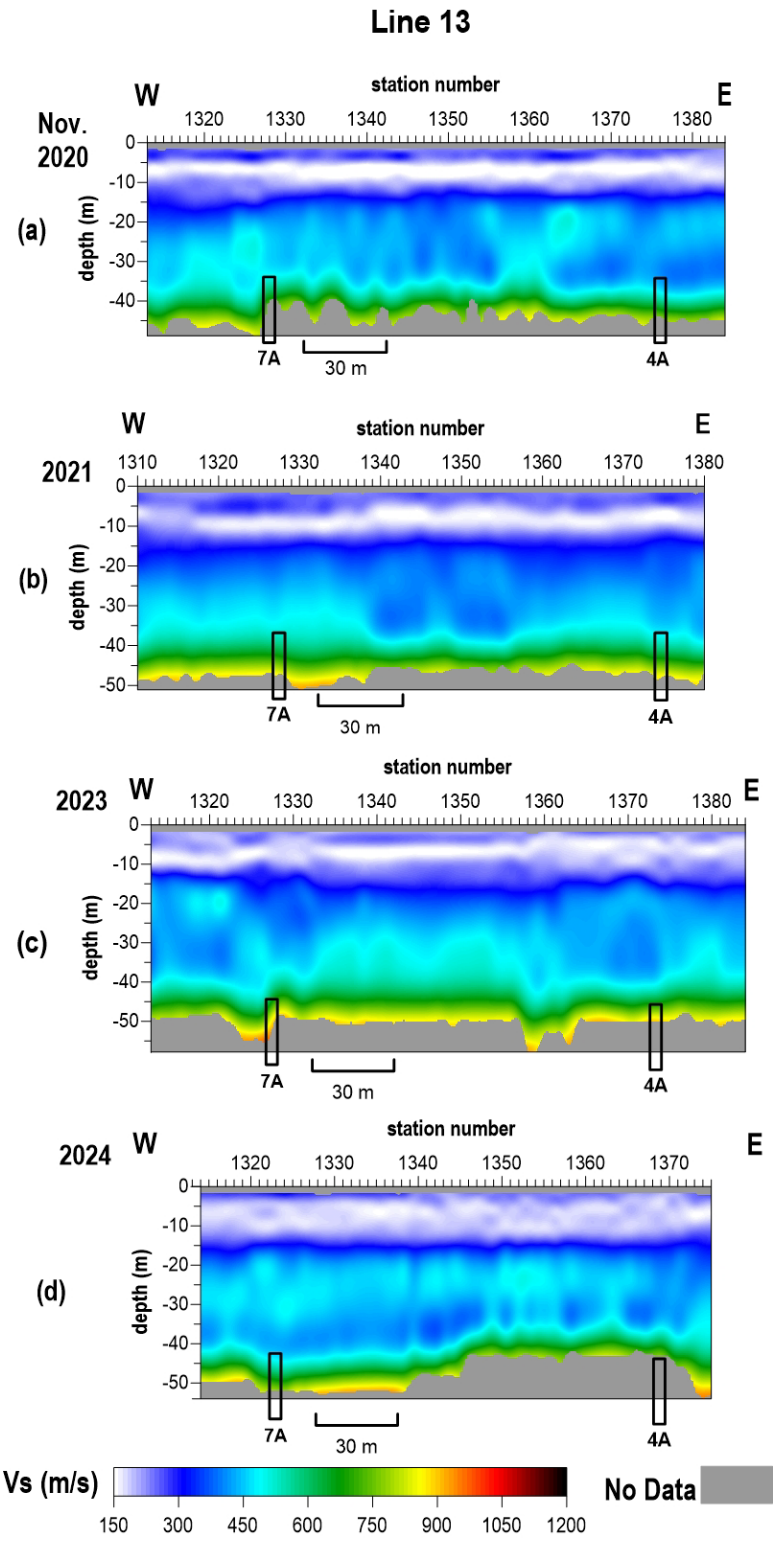

Figure 17. Shear-wave velocity profiles from line 13 from (a) November 2020, (b) November 2021, (c) March 2023, and (d) August 2024 investigation.

Line 14

Line 14 is oriented W-E and extends across wells 3B and 1B, which are approximately located at stations 1430 and 1450 respectively (Figure 18). The 2024 results are similar to the past surveys, but with slight increased depth of investigation due to improved S/N at low frequencies near the east end of the line. The 2023 survey had an apparent pull down in the top of bedrock between stations 1035-1045, likely a result of variability in the inversion layer model caused by the reduced investigation depth (data artifact). Overall bulk velocity profiles suggest a normal stress regime.

Line 15

Line 15 is orientated NW-SE over wells 19, 20, 25, 26, 33, 36, and 94 (Table 5). This line was a new addition to the passive monitoring survey in 2021 and spans a portion of a 2-D profile recorded during a 2010 passive surface wave survey. The overall bulk velocity trend in 2023 for line 15 (Figure 19) is largely consistent with the 2021 and 2010 surveys (Figure 20) with only subtle (~15%) variability. Considering the plugged status of the wells along the railroad tracks, the velocity profile and apparent variability year to year between wells 25 and 94 represents normal variability in the estimated shear velocity.

In the 2023 survey, there was a subtle discontinuity near the top of bedrock at 20-25 m depth between wells 19 and 20. Dispersion curves for stations around the collapsed salt jug show lower and less coherent fundamental mode energy compared to stations where the receiver spread was fully away from the feature (Figure 21). Higher mode energy is observed in the overtone image near the collapse feature at frequencies between 5.5 Hz and 6.5 Hz (Figure 21a). A representative dispersion curve where the spread is fully outside the surface expression exhibits a single fundamental mode trend that is coherent over relevant frequencies (Figure 21b). This multimode behavior supports the suggestion that multimode dispersion patterns may be an indication of heterogeneities at depth for wells over salt jugs that have not migrated to the surface. The apparent velocity discontinuity near the top of bedrock is likely a result of uncertainty in picking the fundamental mode due to the presence of the higher mode. Consistency across the top of bedrock in 2024 supports that interpretation.

Table 5. Wells and corresponding station numbers across line 15.

Well	19	20	25	26	33	36	94
Station No.	15025	15058	15080	15123	15138	15174	15207

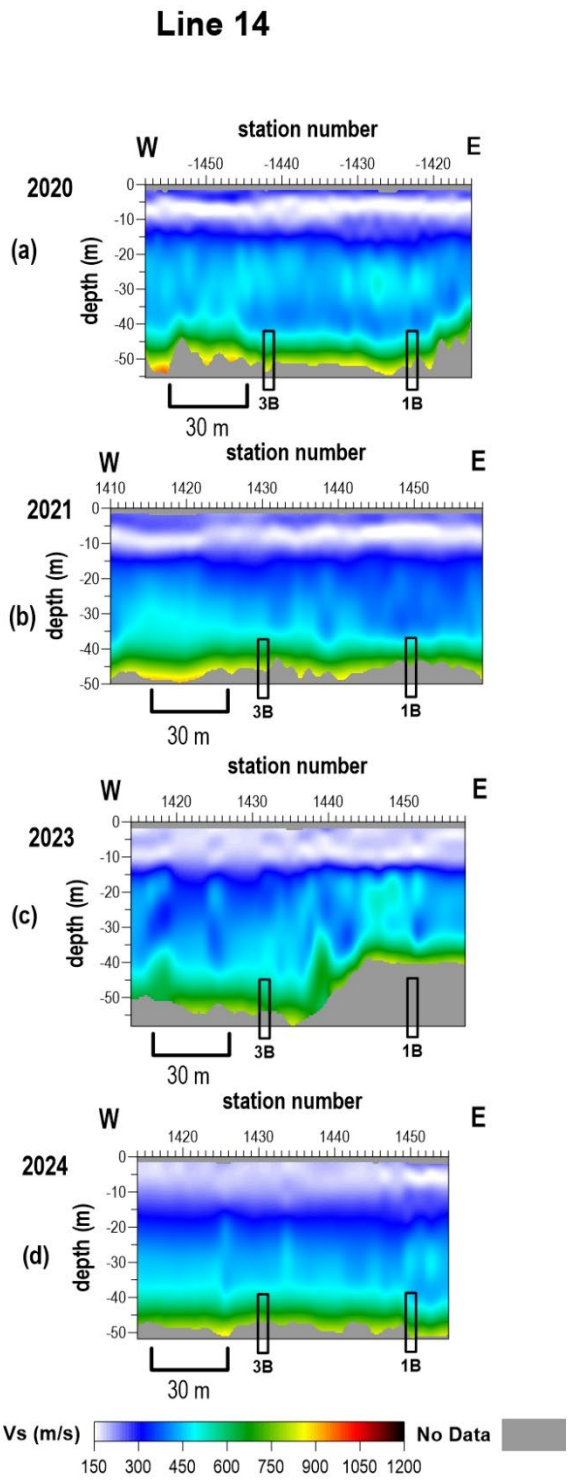

Figure 18. Shear-wave velocity profiles from line 14 from (a) November 2020, (b) November 2021, (c) March 2023, and (d) August 2024 survey.

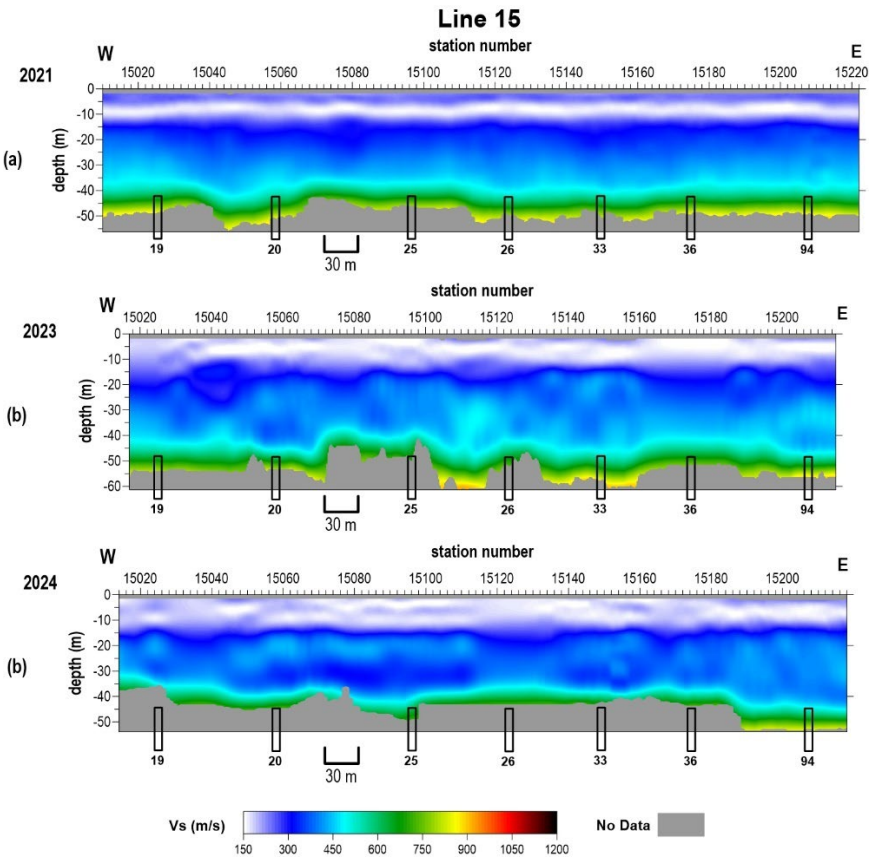

Figure 19. Shear-wave velocity profile from line 15 from (a) November 2021, (b) March 2023 and (c) August 2024.

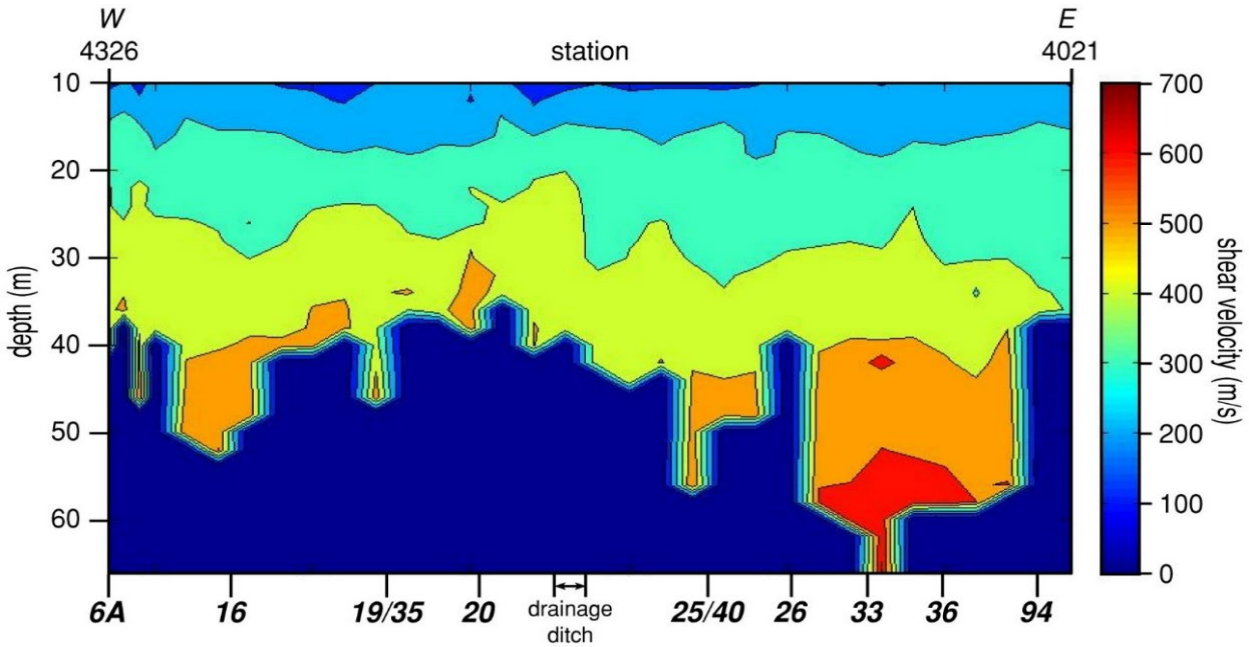

Figure 20. Shear wave velocity profile from the 2010 survey over the location of line 15 in the current survey.

(a) Station 15028

(b) Station 15146

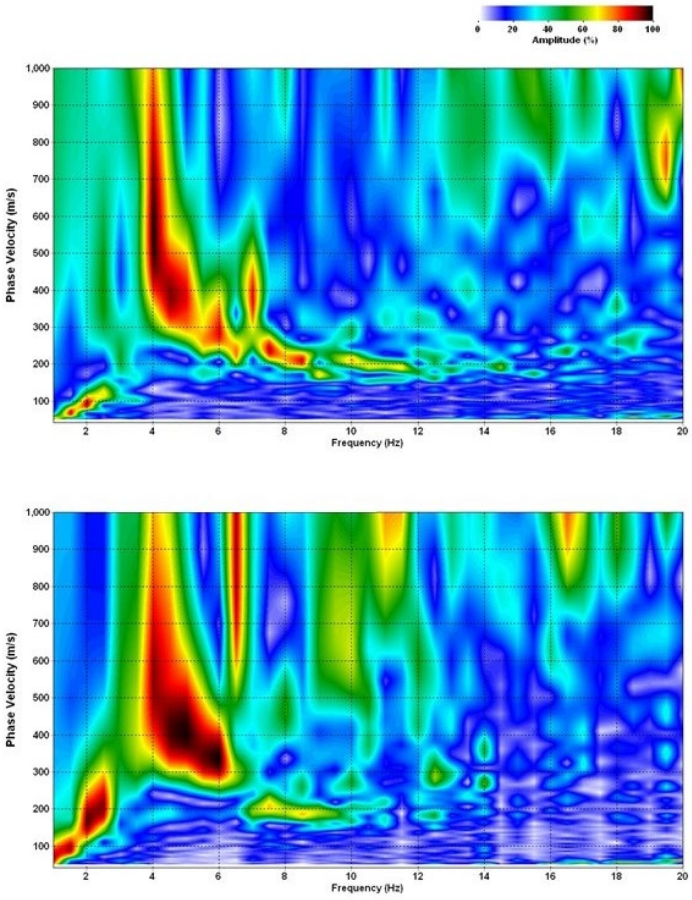

Figure 21. Representative dispersion curves (a) over low velocity anomaly and (b) towards the middle of line 15 from 2023.

Interpretation and Discussion

Wells interpreted with normal or currently stable stress regime (little to no recent timelapse variability)

Wells 1B, 3B, 4A, 6B*, 7A, 7B*, 8B, 10B, 11B, 13B, 15B, 17, 18, 19, 20, 23, 23B, 25, 26, 29, 30, 33, 36, 39, 41, 42, 44, 45, 46, 59, 60, 87, 88, 89, 90, 92, and 94.

* Results from line 12 were artifact-rich and uninterpretable in 2024. Given the historically minimal timelapse variability on this line, conditions at wells 6B and 7B are likely stable.

Wells with recent timelapse variability, but interpreted as currently normal/stable stress regime

Wells 52, 53 (line 9, Williams Street)

The velocity gradient in the upper 30 m of the Williams Street line (line 9) has been reasonably consistent since the beginning of timelapse passive surface wave monitoring. Velocity trends below 30 m have varied slightly over time and have typically been elevated compared to other lines at the CBRA. In 2021, either shear stress or bedrock velocity appeared higher along this line. In 2023, velocities below 30 m remain elevated on the northern half of the line (spanning wells 52 and 53) and decreased on the southern half of the line (spanning wells 59 and 60). In 2024, velocities on the northern half of the line decreased and are consistent with the south half of the line. These observations may suggest dynamic processes at depth (possibly localized failure and redistribution of stress at wells 52 and 53, possibly suggestive of the presence of a gallery—especially considering the static nature of the most resent sonar in well 53. Currently, the velocity profile at line 9 is consistent with elsewhere at this site, likely indicative of a current period of relative stability.

Wells 14B (line 5)

A dome-shaped area of elevated velocity appeared west of well 14B in 2021. Although velocity returned to normal at this location in 2023, the velocity at well 14B was slightly elevated with a subtle velocity halo east of well 14B. Timelapse observations at this well over the past few years suggest dynamic stress changes have occurred that could be associated with changes in the roof structures/characteristics of the salt jug. In 2024, the velocity profile at this well is consistent with the rest of this line, suggesting redistribution of stress and relative stability.

Wells 22A (line 3)

An area of elevated velocity was observed between wells 17 and 42 (line 1) and 45 and 22A (line 3) in 2020. In 2021 and 2023, the overall velocity trend was more consistent with 2019, with a more uniform profile between wells on lines 1 and 3 with only subtle velocity hallows near wells 17 and 42. A 30 m dome-shaped area of elevated velocity observed near well 22A is observed in 2023 and is worth monitoring in future surveys. In general, these observations are consistent with the dynamics these wells have demonstrated in years past and the absence of an anomaly at well 22A in 2024 suggests relative stability at the time of the survey. This level of stress variability is likely characteristic of some jugs due to geometry, depth, or volume. As long as the stress field above the dolomite at 70 m periodically returns to a more ‘normal’ state with no apparent

structural abnormality then the observed dynamics are likely associated with strain at jug depths and not dramatically affecting the bulk strength of the overburden.

Wells with recent timelapse variability and possibly elevated stress

Wells 2A and 4B

Similar to previous years, multi-mode dispersion curves were observed in 2024 near well 2A along line 10, potentially indicative of heterogeneities below the imaging depth of these data. Velocity on line 10 is elevated relative to previous years. Similar to past years, azimuthal variation in bedrock velocity (anisotropy) (between lines 10 and 11) is again observed in 2024. These timelapse changes and velocity anisotropy on lines 10 and 11 suggest the possibility of dynamic stress changes. It is not clear from these data how much strain can be suggested to have occurred beyond the elastic/plastic boundary from these stress observations alone.

Wells 87 and 88 (line 4)

The velocity profile along line 4 is slightly elevated in 2024 at locations that have historically been consistent with expected 'normal' velocities at this site. An area of slightly increased depth of investigation was observed between wells 87 and 88 in 2024. Velocities between these wells are elevated at low frequencies, contributing to longer wavelengths and, thus, increased depth of investigation. Due to low signal-to-noise in this area, it is unclear whether the apparent velocity increase is due to a true increase or a result of interference from higher mode surface wave energy. This anomalous feature is consistent using multiple passive sources and, therefore, warrants attention and additional scrutiny in future annual monitoring surveys.

Conclusions and Recommendations

The shear-wave velocity directly over or in proximity to the majority of wells in this 2024 study continues to represent natural geologic conditions and a normal stress regime. Based on nearly a decade of passive seismic monitoring at most of these wells, shear-wave velocity profiles are classified into three different categories: (1) wells with normal or currently stable stress regime (little to no recent timelapse variability), (2) wells with recent timelapse variability, but interpreted as currently normal/stable stress regime, or (3) wells with recent timelapse variability and possibly elevated stress. Anomalous shear-wave velocity profiles from eight wells are sufficiently outside the normal range to justify an elevated awareness and focused monitoring with enhanced analysis on future surveys.

Strength characteristics estimated from shear-wave velocities derived from the passive MASW surveys around wells 2A and 4B (line 10); 87 and 88 (line 4); 52, 53 (line 9 along Williams Street) 14B (line 5); and 22A (line 3) have changed from historical surveys and are suggestive of possible increases and/or changes in stress due to unstable spans of roof rock above voids. Voids associated with these eight wells currently represent the only apparent potential for void migration toward the ground surface and thereby affecting the stability of material above the bedrock surface in the survey area. In general, with current conditions largely reflecting normal or stable stress regimes with only a few areas possessing subtle and relatively minimally elevated stress, continued monitoring is recommended on an annual basis.

References

Dellwig, L.F., 1963, Environment and mechanics of deposition of the Permian Hutchinson Salt Member of the Wellington shale: Symposium on Salt, Northern Ohio Geological Society, p. 74-85.

Dvorkin, J., A. Nur, and C. Chaika, 1996, Stress sensitivity of sandstones: *Geophysics*, v. 61, p. 444-455.

Eberhart-Phillips, D., D.-H. Han, and M.D. Zoback, 1989, Empirical relationships among seismic velocity, effective pressure, porosity, and clay content in sandstone: *Geophysics*, v. 54, p. 82-89.

Holdoway, K.A., 1978, Deposition of evaporites and red beds of the Nippewalla Group, Permian, western Kansas: Kansas Geological Survey Bulletin 215.

Ivanov, J., R.D. Miller, S.L. Peterie, J.T. Schwenk, J.J. Nolan, B. Bennett, B. Wedel, J. Anderson, J. Chandler, and S. Green, 2013, Enhanced passive seismic characterization of high priority salt jugs in Hutchinson, Kansas: Preliminary report to Burns & McDonnell Engineering Company.

Khaksar, A., C.M. Griffiths, and C. McCann, 1999, Compressional- and shear-wave velocities as a function of confining stress in dry sandstones: *Geophysical Prospecting*, v. 47, p. 487-508.

Kulstad, R.O., 1959, Thickness and salt percentage of the Hutchinson salt; *in* Symposium on Geophysics in Kansas: Kansas Geological Survey Bulletin 137, p. 241-247.

McGuire, D., and B. Miller, 1989, The utility of single-point seismic data; *in* Geophysics in Kansas, D.W. Steeples, ed.: Kansas Geological Survey Bulletin 226, p. 1-8.

Merriam, D.F., 1963, The Geologic History of Kansas: Kansas Geological Survey Bulletin 162, 317 p.

Merriam, D.F., and C.J. Mann, 1957, Sinkholes and related geologic features in Kansas: *Transactions of the Kansas Academy of Science*, v. 60, p. 207-243.

Miller, R.D., 2011, Progress report: 3-D passive surface-wave investigation of solution mining voids in Hutchinson, Kansas: Interim report to Burns & McDonnell Engineering Company, January, 9 p.

Miller, R.D., J. Ivanov, S.D. Sloan, S.L. Walters, B. Leitner, A. Rech, B.A. Wedel, A.R. Wedel, J.M. Anderson, O.M. Metheny, and J.C. Schwarzer, 2009, Shear-wave study above Vigindustries, Inc. legacy salt jugs in Hutchinson, Kansas: Kansas Geological Survey Open-file Report 2009-3.

Park, C., R. Miller, D. Laflen, N. Cabrillo, J. Ivanov, B. Bennett, and R. Huggins, 2004, Imaging dispersion curves of passive surface waves [Exp. Abs.]: Annual Meeting of the Soc. of Expl. Geophys., Denver, Colorado, October 10-15, p. 1357-1360.

Sayers, C.M., 2004, Monitoring production-induced stress changes using seismic waves [Exp. Abs.]: Annual Meeting of the Soc. of Expl. Geophys., Denver, Colorado, October 10-15, p. 2287-2290.

Sloan, S.D., S.L. Peterie, J. Ivanov, R.D. Miller, and J.R. McKenna, 2010, Void detection using near-surface seismic methods; *in* Advances in Near-Surface Seismology and Ground-Penetrating Radar, SEG Geophysical Developments Series No. 15, R.D. Miller, J.D. Bradford, and K. Holliger, eds.: Tulsa, Society of Exploration Geophysicists, p. 201-218.

Swineford, A., 1955, Petrography of upper Permian rocks in south-central Kansas: State Geological Survey of Kansas Bulletin 111, 179 p.

Walters, R.F., 1978, Land subsidence in central Kansas related to salt dissolution: Kansas Geological Survey Bulletin 214, 82 p.

Whittemore, D.O., 1989, Geochemical characterization of saltwater contamination in the Macksville sink and adjacent aquifer: Kansas Geological Survey Open-file Report 89-35.

Whittemore, D.O., 1990, Geochemical identification of saltwater contamination at the Siefkes subsidence site: Report for the Kansas Corporation Commission.

Appendix

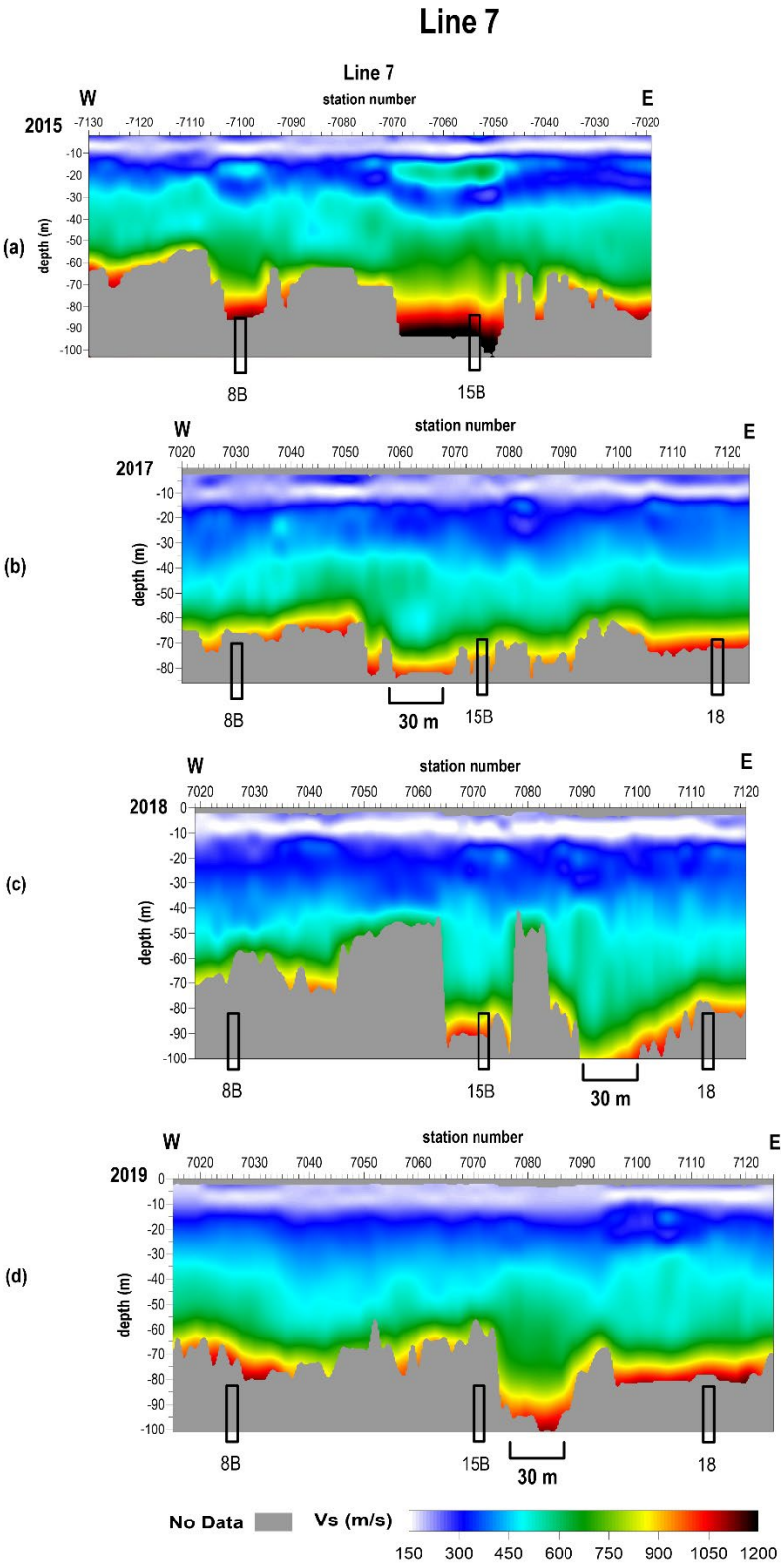

Figure A-1. Shear wave velocity profiles from line 7 in proximity to well 15B for 2015-2019.

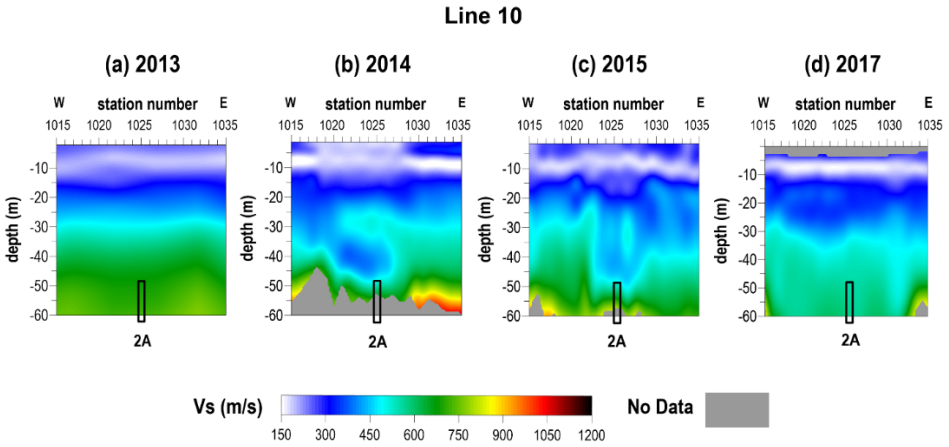

Figure A-2. Shear wave velocity profiles for line 10 over well 2A for 2013-2017.